PHYSICAL REVIEW B **90**, 201202(R) (2014)

Quantum oscillations in Rashba semiconductor BiTeCl

F. Chen,[1] D. Zhao,[1] Z. J. Xiang,[1] C. Shang,[1] X. G. Luo,[1] B. Y. Pan,[2] S. Y. Li,[2] T. Wu,[1,*] and X. H. Chen[1,†]

[1]*Hefei National Laboratory for Physical Science at Microscale and Department of Physics, University of Science and Technology of China, Hefei, Anhui 230026, People's Republic of China*

[2]*State Key Laboratory of Surface Physics, Department of Physics, and Laboratory of Advanced Materials, Fudan University, Shanghai 200433, China*

(Received 26 August 2014; revised manuscript received 16 October 2014; published 10 November 2014)

Recently, a Dirac surface state (SS) was observed in Rashba semiconductor BiTeCl by angle-resolved photoemission spectroscopy (ARPES), which suggested strong inversion symmetry breaking therein, despite the absence of such symmetry breaking in existing first-principles calculations. To clarify the aforementioned conflict as well as understand the nature of such emergent phenomenon, we employ both high-field Shubnikov–de Haas (SdH) oscillation and Hall measurements to study BiTeCl single crystals. Both techniques yield consistent observation of a three-dimensional Fermi surface from a bulk state, while Dirac surface state contribution appears absent. Finally, we propose that various gating techniques could be used to explore the novel topological nature of this material.

DOI: 10.1103/PhysRevB.90.201202 PACS number(s): 71.18.+y, 71.20.−b, 71.70.Ej

Topological insulators (TIs) are one kind of newly discovered quantum materials with a novel quantum state in condensed matter physics, which exhibits an insulating bulk state and a time-reversal symmetry protected metallic surface/edge state due to spin-orbital interaction (SOI) [1,2]. Most topological insulators discovered so far preserve lattice inversion symmetry [1–3] except for strained HgTe [4], which weakly breaks the inversion symmetry due to its zinc-blende structure. Since inversion asymmetric topological insulators (IATIs) would lead to many interesting topological phenomena and practical applications, including crystalline-surface-dependent topological electronic states, pyroelectricity, and intrinsic topological *p*-*n* junctions [5], the search for IATIs has attracted a lot of interest and efforts in recent research.

Rashba semiconductor BiTeX (X = I, Br, Cl), which possesses both a strong atomic SOI and inversion asymmetric bulk structure, could be a potential candidate for IATIs. However, giant Rashba-type spin splitting (RSS) is widely found in these materials instead of TI phase. This is also confirmed by first-principles calculations [6]. Although recent first-principles calculations found that a TI phase could be achieved in BiTeI under pressure [7] and a possible topological quantum phase transition has been suggested by recent high-pressure infared and Raman spectra experiments [8,9], the TI phase under high pressure is still controversial [8,9]. Whether TI phase can be achieved in Rashba semiconductor BiTeX is still an open issue. Very recently, a Dirac surface state (SS) was discovered by angle-resolved photoemission spectroscopy (ARPES) experiments in BiTeCl single crystals [5], which also belong to the same Rashba semiconductor family as BiTeI. This result supports a strong inversion asymmetric TI phase even without external high pressure. This is completely out of the expectation from first-principles calculations [6]. How to understand the emergence of this unexpected TI phase in this material becomes an open issue. Here, we use both Hall effect and Shubnikov–de Haas (SdH) quantum oscillation to study the Fermi surface (FS) in BiTeCl single crystals. Both techniques give a consistent result on a three-dimensional (3D) FS of bulk state and there is no trace of a Dirac SS in the present experiment. These results could be used to reconcile previous theoretical results with recent ARPES experiments, suggesting that the Dirac SS observed by recent ARPES should be caused by surface-related effect rather than the usual bulk-to-surface correspondence in topological insulators.

A BiTeCl single crystal was synthesized by a self-flux method [10]. The precursor, Bi_2Te_3 polycrystal, weighted according to stoichiometric ratio was heated to 873 K and kept for 24 hours before shutting off the furnace. After that, the mixture of Bi_2Te_3 and $BiCl_3$ with the mole ratio of 1:9 was weighted and thoroughly ground, and the mixture was loaded into an alumina crucible before being sealed into an evacuated quartz tube. Then the entire mixture was heated to 723–873 K, kept for 48 hours, and slowly cooled to 473 K for 8 days. Finally the furnace is shut off to room temperature. All the sample processing procedures are performed in a glovebox filled with argon atmosphere. The photograph of a BiTeCl single crystal with several mm^2 area is shown in the inset of Fig. 1(c). The samples were characterized by x-ray diffraction (XRD) using a Rigaku D/max-A x-ray diffractometer with Cu $K\alpha$ radiation in the range of 5°–70° with the step of 0.01° at ambient temperature, and the crystal parameter c = 12.391 Å is obtained, which agrees with previous report [11]. The actual Bi, Te, and Cl concentration of the single crystals was determined from energy dispersive spectroscopy (EDS) analysis as 1:0.99:0.92, suggesting slight nonstoichiometry in our samples.

Temperature-dependent resistivity and Hall effect of BiTeCl single crystals are shown in Fig. 1(d). Due to non-stoichiometry, a metallic behavior instead of semiconducting behavior is observed, consistent with previous transport results [12]. Meanwhile, temperature-independent Hall effect reveals an *n*-type carrier doping with a carrier density (n_{Hall}) of about 7.18×10^{18} cm^{-3}, indicating a Fermi level crossing the bulk conduction band (BCB) as shown in Fig. 1(b). Furthermore, the calculated Hall mobility at 2 K is about 259 cm^2 V^{-1} s^{-1}. Samples with lower carrier density could also be obtained

*wutao@ustc.edu.cn
†chenxh@ustc.edu.cn

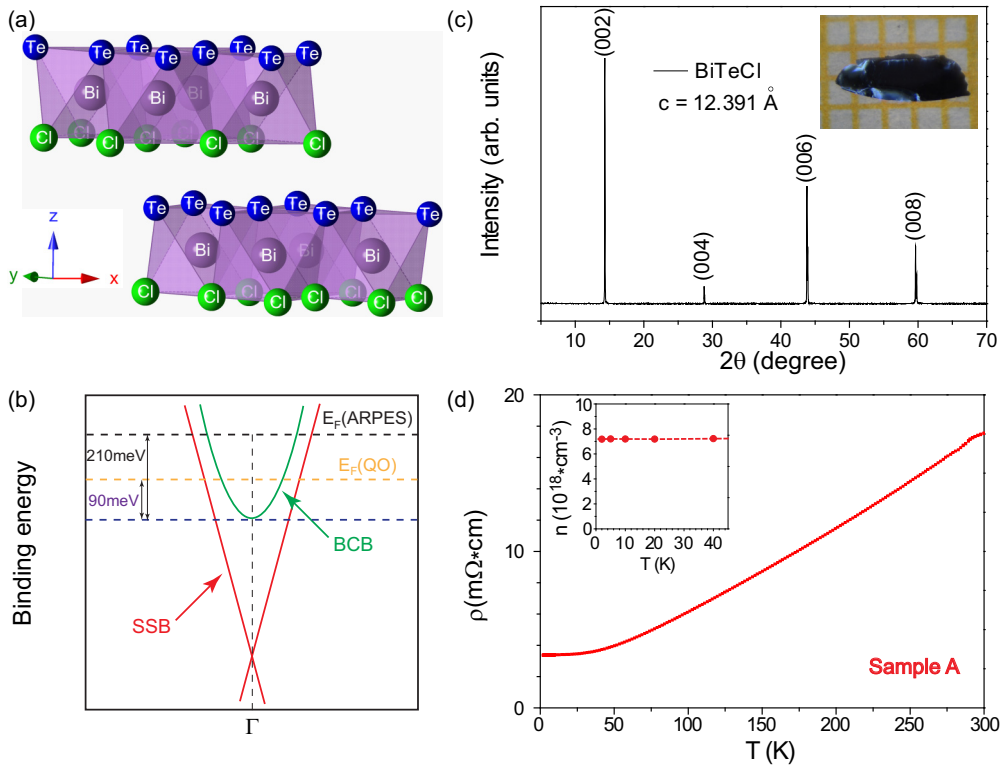

FIG. 1. (Color online) (a) The crystal structure of BiTeCl with P_{63mc} space group. (b) The Fermi level of BiTeCl decided by ARPES [E_F(ARPES)] [5] and quantum oscillation [E_F(QO)], respectively. Here QO stands for the quantum oscillation. The Fermi levels are equal to the distance between two dashed lines with the black and yellow colors and the bottom of the conduction band, which are 210 and 90 meV, respectively. (c) XRD pattern of the BiTeCl single crystal. The inset is the photograph of the BiTeCl single crystal. (d) The temperature-dependent resistivity of BiTeCl. The inset is the n-type carrier concentration decided by Hall measurement.

from the same crystal-growth procedure as the above samples. Although the carrier density varies between different samples, n-type carrier doping does not change. We will discuss the lower-carrier-density samples later. Next, we will first show our magnetoresistance results on the higher-carrier-density samples.

Figure 2(a) shows the typical magnetoresistance at 2 K with a magnetic field as high as 14 T. The corresponding derivative dR/dB exhibits quantum oscillation behavior as shown in Fig. 2(b). Single oscillation frequency (F) 147 T is resolved by fast Fourier transformation (FFT) as shown in the inset of Fig. 2(b). By calculating $F = (\hbar c/2\pi e)S_F$ and $S_F = \pi k_F^2$, where $\hbar$ is the Planck constant, S_F is the Fermi surface area, and k_F is the Fermi level crossing in momentum space, we could obtain $k_F = 0.0667$ Å^{-1}. Besides checking the high-field part of magnetoresistance for quantum oscillation, we also check the low-field part of mangetoresistance for possible weak antilocalization (WAL) effect, which is widely observed in TI due to SOI and disorder effect. A cusp of magnetoresistance at zero field is the main characteristic for WAL effect in magnetoresistance, which is well described by the Hikami-Larkin-Nagaoka (HLN) model [13,14]. According to measurements down to 60 mK as shown in Fig. 2(d), the evidence for WAL in this system is negative.

In order to find out whether the observed SdH quantum oscillation is from the topological SS or bulk state, we also measured angular dependent quantum oscillations. Since the topological SS should exhibit a two-dimensional (2D) FS, the angular dependent oscillation frequency of topological SSs should follow $F(\theta) = F_0/\cos(\theta)$, where θ is the angle between the magnetic field direction and the c axis as shown in Fig. 3(d). However, for an ideal 3D bulk state, the corresponding angular dependent oscillation frequency should be angular independent. In layered 3D materials, the angular dependent oscillation frequency would show a weak angular dependence but much less than that of the 2D case. This difference could be used to distinguish the contributions of 2D and 3D FSs. By analyzing the angular dependent quantum oscillation in Fig. 3(c), we obtain the relationship between the oscillation frequency and the rotation angle, as shown by the black circles in Fig. 3(d). With increasing rotating angle, the angular dependent oscillation frequency deviates from the behavior of the 2D FS and becomes apparent at larger angles. It definitely excludes the possible origin of topological SSs for the observed quantum oscillation. On the other hand, the observed behavior is actually very similar to that of the bulk FS in Bi_2Se_3 [15–17], which possesses a similar layered structure to BiTeCl [Fig. 1(a)]. This indicates that the observed quantum oscillation is from the contribution of the 3D bulk state. Thus, for the 3D FS, the carrier concentration $n = k_F^3/3\pi^2$ corresponding to the quantum oscillation is about 9.7×10^{18} cm^{-3}, which is quite consistent with that of the Hall measurement. Furthermore, we have also measured the temperature-dependent quantum oscillation as shown in Fig. 3(a). According to the Lifshitz-Kosevich formula [18], the amplitude of the quantum oscillation for certain FSs is correlated with the temperature

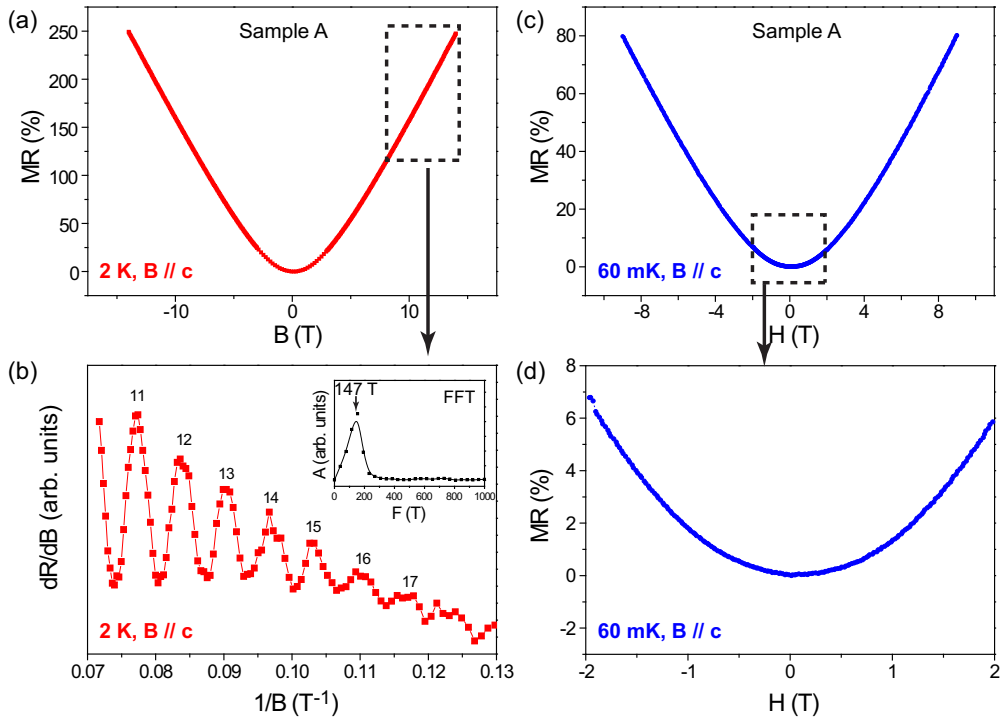

FIG. 2. (Color online) (a) The magnetoresistance with magnetic field applied along the c-axis direction at 2 K. (b) The derivative dR/dB corresponding to the magnetoresistance in the dashed rectangle of panel (a). The number on each peak of the derivative corresponds to Landau level index n, and the inset is the FFT of the quantum oscillation. (c) c-axis magnetoresistance at 60 mK. (d) Low-field blow-up plot of (c).

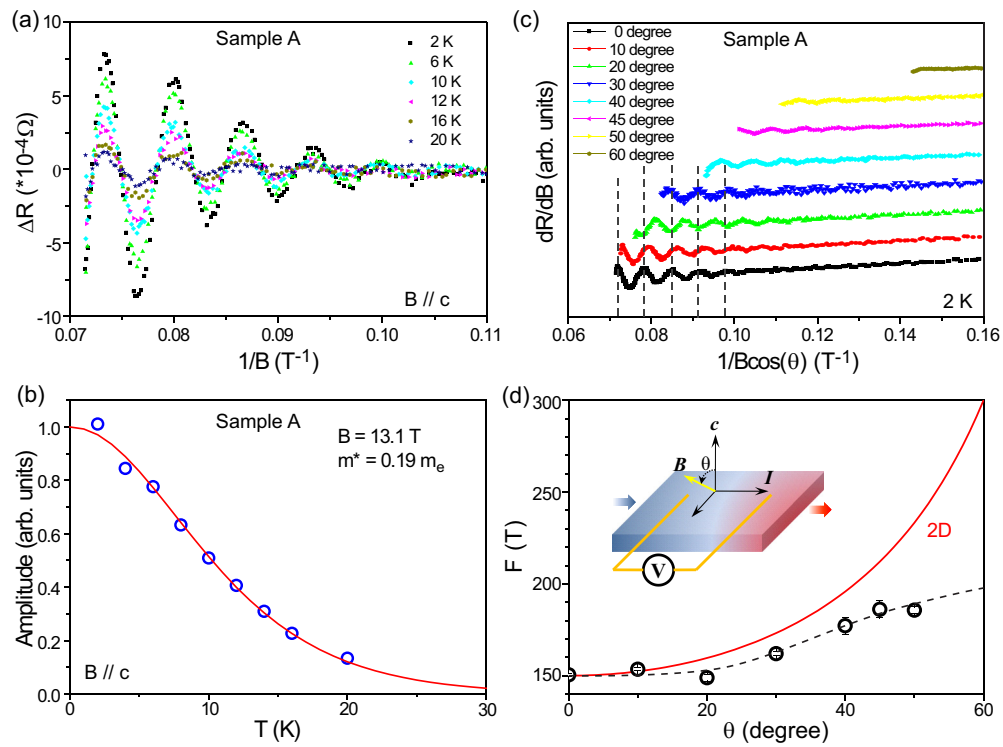

FIG. 3. (Color online) (a) T-dependent amplitudes of SdH quantum oscillation with a magnetic field applied along the c-axis direction of the sample. (b) T-dependent amplitude of quantum oscillation at $B = 13.1$ T. The blue circle is the amplitude decided by the data in panel (a), and the solid red line is the fitting result. (c) Angular dependent quantum oscillation at 2 K. (d) Angular dependent quantum oscillation frequency. The red line describes the angular dependent quantum oscillation frequency of the 2D Fermi surface, and the black circles are the experimental results decided from the slope of Landau-level index n versus $1/B$ in panel (c). The dashed line is a guide for the eyes. The inset is the measurement configuration. θ is the rotation angle between the c-axis direction and the direction of the magnetic field. All the transport parameters obtained from the SdH oscillation analysis are given in Table I.

TABLE I. The transport parameters obtained from the SdH oscillation analysis with formula $v_F = \hbar k_F/m^*$, $\tau = \hbar/2\pi k_B T_D$, $l_{QO} = v_F\tau$, and $\mu = e\tau/m^*$.

F (T)	k_F (Å^{-1})	n_{QO} ($\times 10^{19}$ m^{-3})	v_F ($\times 10^5$ ms^{-1})	m^* (m_e)
147	0.0667	0.97	4.02	0.19
E_F (meV)	T_D (K)	τ ($\times 10^{-14}$ s^{-1})	l_{QO} ($\times 10^{-8}$ m)	μ (cm^2 V^{-1} s^{-1})
90	29.9	4.06	1.63	376

and magnetic field as $A(T,B) \propto B^{-1/2} * \exp(-\alpha m^* T_D/B) * (\alpha m^* T/B)/\sinh(\alpha m^* T/B)$, where $A(T,B)$ is the amplitude of quantum oscillation, $\alpha = 2\pi^2 k_B/e\hbar \approx 14.69$ Tesla/K, the effective mass $m^* = m * m_e$, and T_D is the Dingle temperature. By fitting the relation between the amplitude and the temperature at a certain magnetic field, $A(T) = A_0(\alpha m^* T/B)/\sinh(\alpha m^* T/B)$, where A_0 is a constant, we could obtain the effective mass $m^* = 0.19 m_e$ as shown in Fig. 3(b). The effective mass for BCB from recent ARPES experiments is about $0.235 m_e$ [5]. These two values show good agreement. Using the above effective mass, we could also calculate the Fermi level relative to the conduction band bottom with $E_F = \hbar^2 k_F^2/2m^*$ and the corresponding E_F is about 90 meV. Table I shows a complete list of physical parameters derived from the analysis of temperature-dependent SdH quantum oscillation. Among them, $T_D = 29.9$ K could be determined from the slope of the Dingle plot at certain temperatures with formula $\ln[AB^{1/2}\sinh(\alpha m^* T/B)] = \text{const} - \alpha m^* T_D/B$. It should be mentioned that the mobility from quantum oscillation is also comparable with that from Hall effect. Thus, all these results strongly support bulk origin for the observed SdH quantum oscillation. Compared with recent ARPES experiments on BiTeCl as shown in Fig. 1(b), the bulk Fermi level determined in the present study is much lower than the Fermi level from ARPES measurements. Although there are some discrepancies between early and recent ARPES experiments [5,10,19], it does not change this conclusion. This could be ascribed to band bending near the surface region due to surface polarity in this material, which is well known in Rashba semiconductor BiTeX [6,10,12,19–22].

The absence of 2D topological SS evidence in our BiTeCl samples with high carrier density could be caused by a large residual bulk contribution which masks the surface contribution in transport measurement. One way to suppress the bulk contribution is to reduce the carrier density in the bulk. As we discussed before, we could obtain some BiTeCl single crystals with relatively lower carrier density from the same crystal-growth procedure as samples with higher carrier density. We have also measured both temperature-dependent resistivity and Hall effect for these samples as shown in Fig. 4. The amplitude of resistivity at 2 K is enhanced more than one order of magnitude for these samples with lower carrier density as shown in Fig. 4(a). Meanwhile, the carrier density is reduced by about five times compared with high-carrier-density samples as shown in Fig. 4(b). Moreover, a weak insulating behavior is also observed below 50 K in resistivity for the low-carrier-density samples. This could be ascribed to the formation of mobility edge. Due to nonstoichiometry, the carrier doping would also lead to disorder effect and a

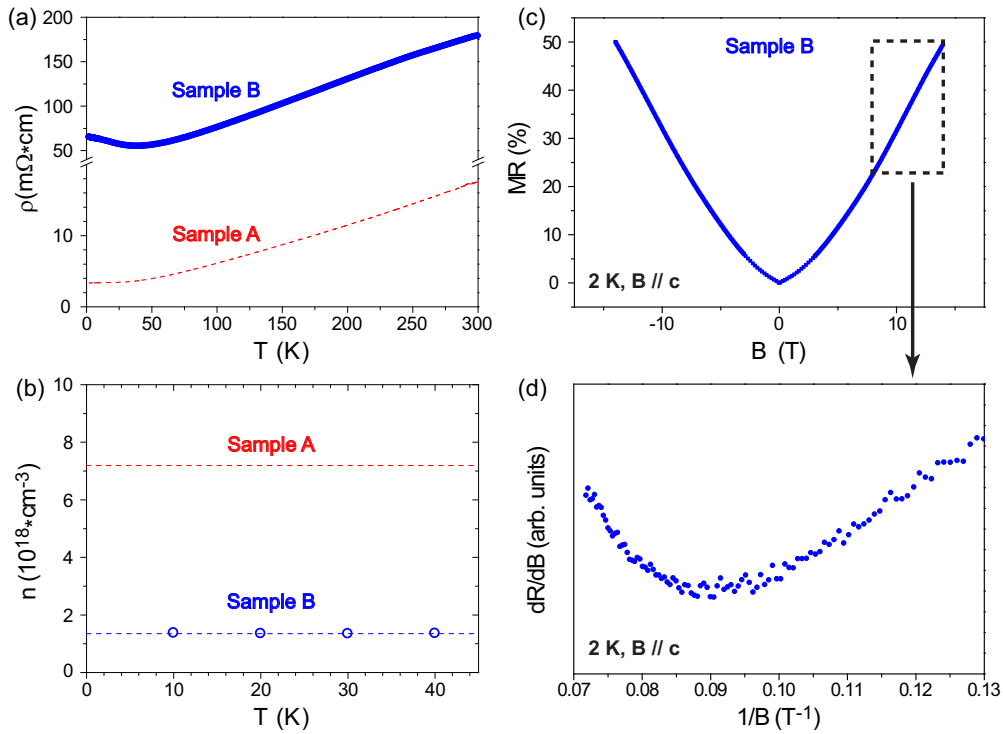

FIG. 4. (Color online) (a) The temperature-dependent resistivity of BiTeCl. (b) The n-type carrier concentration decided by Hall measurement. The red dashed line corresponds to the data in Fig. 1(d). (c) The magnetoresistance with magnetic field applied along the c-axis direction at 2 K. (b) The derivative dR/dB corresponding to the magnetoresistance in the dashed rectangle of panel (d).

mobility edge is formed close to the bottom of the conduction band due to weak localization effect. As the carrier density is higher, the Fermi level is always higher than the mobility edge and there is no observed localization effect in charge transport. As the carrier density is reduced, the Fermi level would finally fall below the mobility edge and the system will exhibit localization effect at low temperature. This is also useful to diminish the bulk contribution in transport. We also calculate the Hall mobility for these low-carrier-density samples and its value is about 71 $cm^2\ V^{-1}\ s^{-1}$, much smaller than that of the high-carrier-density samples. This result also supports the fact that the Fermi level in our low-carrier-density samples falls below the bulk mobility edge. Therefore, these samples are expected to be better for studying possible 2D topological SSs. However, as shown in Fig. 4(c), we still have not found any trace of a 2D surface conduction channel on such BiTeCl single crystals as expected in magnetoresistance measurements. Since the bulk mobility is also reduced in these samples, even quantum oscillation from the bulk state is also absent in these samples as shown in Fig. 4(d).

At the present stage, our results do not support the existence of a 2D topological SS in BiTeCl single crystals, which agrees with previous first-principles calculations though a high-field experiment is also needed to search for possible 2D topological SSs. One possible way to reconcile the absence of topological SSs in the present transport with recent ARPES results is to consider surface-related effect. Due to the strong covalency and ionicity of Bi-Te and Bi-I bonds, respectively, the bulk crystal of BiTeCl intrinsically possesses a polar axis along the *c*-axis direction. This would lead to a strong surface polarity in this material. In fact, surface polarity effect has already been considered in recent ARPES experiments to understand the unexpected Dirac SS, in which surface polarity is believed to generate a large effective pressure ($\sim 10^9$ Pa) along the *c*-axis direction and thus drives the crystal (possibly the several top layers) into the topological insulator phase as suggested by Bahramy *et al.* in BiTeI under hydrostatic pressure [5,7]. ARPES measurement is conducted under high vacuum and this is important to preserve surface polarity. However, in transport measurement of bulk single crystals, the surfaces are always passivated and the surface polarity is compensated by various surface adsorption. It is possible that the left uncompensated surface polarity on the passivated surface in our transport measurements is not enough to drive the crystal into a topological insulator phase. Considering the surface polarity as the possible origin of 2D topological SSs, we propose that various gating techniques could be used to play the same role of surface polarity to induce 2D topological SSs in BiTeCl without high vacuum. On the other hand, diminishing bulk contribution is also a necessary step to observe 2D topological SS contribution in transport. Therefore, further study on thin film or flake samples of BiTeCl with an appropriate voltage gating technique (such as liquid gate) would be a way to solve the puzzle of the unexpected 2D topological SS in BiTeCl single crystals.

In the present study, we have measured both Hall effect and SdH quantum oscillation to explore the possible 2D topological SS in BiTeCl single crystals. Both techniques give a consistent result on a three-dimensional FS of bulk state and there is no trace of the Dirac SS even on the low-carrier-density sample with weak localization at low temperature. These results suggest that the Dirac SS in BiTeCl single crystals observed by recent ARPES should be caused by surface-related effect rather than the usual bulk-to-surface correspondence in topological insulators. Considering the surface polarity as the possible origin of 2D topological SSs, we propose that various gating techniques could be used to to explore the novel topological nature of this material.

Note added. Recently, two papers have appeared which also report the SdH quantum oscillation in BiTeCl single crystals [23,24]. The high-field quantum oscillation in Ref. [23] is consistent with our present conclusion on the absence of a 2D topological SS in BiTeCl bulk single crystals.

The authors are grateful for the discussions with Z. Sun and Z. H. Qiao. This work is supported by the National Natural Science Foundation of China (Grant No. 11190021), the "Strategic Priority Research Program (B)" of the Chinese Academy of Sciences (Grant No. XDB04040100), the National Basic Research Program of China (973 Program, Grant No. 2012CB922002), Specialized Research Fund for the Doctoral Program of Higher Education (Grant No. 20133402110032), and the Chinese Academy of Sciences.

[1] M. Z. Hasan and C. L. Kane, Rev. Mod. Phys. **82**, 3045 (2010).
[2] X. L. Qi and S. C. Zhang, Rev. Mod. Phys. **83**, 1057 (2011).
[3] W. A. Phelan, S. M. Koohpayeh, P. Cottingham, J. W. Freeland, J. C. Leiner, C. L. Broholm, and T. M. McQueen, Phys. Rev. X **4**, 031012 (2014).
[4] B. A. Bernevig, T. L. Hughes, and S. C. Zhang, Science **314**, 1757 (2006).
[5] Y. L. Chen, M. Kanou, Z. K. Liu, H. J. Zhang, J. A. Sobota, D. Leuenberger, S. K. Mo, B. Zhou, S. L. Yang, P. S. Kirchmann, D. H. Lu, R. G. Moore, Z. Hussain, Z. X. Shen, X. L. Qi, and T. Sasagawa, Nat. Phys. **9**, 704 (2013).
[6] S. V. Eremeev, I. A. Nechaev, Yu. M. Koroteev, P. M. Echenique, and E. V. Chulkov, Phys. Rev. Lett. **108**, 246802 (2012).
[7] M. S. Bahramy, B.-J. Yang, R. Arita, and N. Nagaosa, Nat. Commun. **3**, 679 (2012).
[8] X. Xi, C. Ma, Z. Liu, Z. Chen, W. Ku, H. Berger, C. Martin, D. B. Tanner, and G. L. Carr, Phys. Rev. Lett. **111**, 155701 (2013).
[9] M. K. Tran, J. Levallois, P. Lerch, J. Teyssier, A. B. Kuzmenko, G. Auts, O. V. Yazyev, A. Ubaldini, E. Giannini, D. van der Marel, and A. Akrap, Phys. Rev. Lett. **112**, 047402 (2014).
[10] G. Landolt, S. V. Eremeev, O. E. Tereshchenko, S. Muff, B. Slomski, K. A. Kokh, M. Kobayashi, T. Schmitt, V. N. Strocov, J. Osterwalder, E. V. Chulkov, and J. Hugo Dil, New. J. Phys. **15**, 085022 (2013).
[11] A. V. Shevelkov, E. V. Dikarev, R. V. Shpanchenko, and B. A. Popovkin, J. Solid State Chem. **114**, 379 (1995).

[12] M. Sakano, M. Bahramy, A. Katayama, T. Shimojima, H. Murakawa, Y. Kaneko, W. Malaeb, S. Shin, K. Ono, H. Kumigashira, R. Arita, N. Nagaosa, H. Hwang, Y. Tokura, and K. Ishizaka, Phys. Rev. Lett. **110**, 107204 (2013).

[13] S. Hikami, A. I. Larkin, and Y. Nagaoka, Prog. Theor. Phys. **63**, 707 (1980).

[14] D. X. Qu, Y. S. Hor, Jun Xiong, R. J. Cava, and N. P. Ong, Science **329**, 821 (2010).

[15] L. Fang, Y. Jia, D. J. Miller, M. L. Latimer, Z. L. Xiao, U. Welp, G. W. Crabtree, and W.-K. Kwok, Nano Lett. **12**, 6164 (2012).

[16] F. M. Qu, C. Zhang, R. R. Du, and L. Lu, J. Low Temp. Phys. **170**, 397 (2013).

[17] A. Wolos, S. Szyszko, A. Drabinska, M. Kaminska, S. G. Strzelecka, A. Hruban, A. Materna, and M. Piersa, Phys. Rev. Lett. **109**, 247604 (2012).

[18] D. Shoenberg, *Magnetic Oscillations in Metals* (Cambridge University Press, Cambridge, 1984).

[19] G. Landolt, S. V. Eremeev, Y. M. Koroteev, B. Slomski, S. Muff, T. Neupert, M. Kobayashi, V. N. Strocov, T. Schmitt, Z. S. Aliev, M. B. Babanly, I. R. Amiraslanov, E. V. Chulkov, J. Osterwalder, and J. H. Dil, Phys. Rev. Lett. **109**, 116403 (2012).

[20] S. V. Eremeev, I. P. Rusinov, I. A. Nechaev, and E. V. Chulkov, New J. Phys. **15**, 075015 (2013).

[21] K. Ishizaka, M. S. Bahramy, H. Murakawa, M. Sakano, T. Shimojima, T. Sonobe, K. Koizumi, S. Shin, H. Miyahara, A. Kimura, K. Miyamoto, T. Okuda, H. Namatame, M. Taniguchi, R. Arita, N. Nagaosa, K. Kobayashi, Y. Murakami, R. Kumai, Y. Kaneko, Y. Onose, and Y. Tokura, Nat. Mater. **10**, 521 (2011).

[22] A. Crepaldi, L. Moreschini, G. Auts, C. Tournier-Colletta, S. Moser, N. Virk, H. Berger, P. Bugnon, Y. J. Chang, K. Kern, A. Bostwick, E. Rotenberg, O. V. Yazyev, and M. Grioni, Phys. Rev. Lett. **109**, 096803 (2012).

[23] C. Martin, A. V. Suslov, S. Buvaev, A. F. Hebard, P. Bugnon, H. Berger, A. Magrez, and D. B. Tanner, arXiv:1407.6739.

[24] F. X. Xiang, X. L. Wang, and S. X. Dou, arXiv:1401.6732.